# A framework to account for structural damage, functional efficiency and reparation costs within the optimal design of countermeasures: Application to snow avalanche risk mitigation

Philomène Favier, Nicolas Eckert, Thierry Faug, David Bertrand, Isabelle Ousset, Gabriel Candia, Juan Carlos de la Llera

# A framework to account for structural damage, functional efficiency and reparation costs within the optimal design of countermeasures: application to snow avalanche risk mitigation

Philomène Favier[1], Nicolas Eckert[2], Thierry Faug[2], David Bertrand[3], Isabelle Ousset[2], Gabriel Candia[4], and Juan Carlos de la Llera[4]

[1]Univ. Grenoble Alpes, INRAE, LESSEM, 38000 Grenoble, France

[2]Univ. Grenoble Alpes, INRAE, ETNA, 38000 Grenoble, France

[3]INSA Lyon, SMS-ID Laboratory, 69621 Villeurbanne Cedex, France

[4]CIGIDEN, National Research Center for Integrated Natural Disaster Management, and Pontificia Universidad Católica de Chile, Santiago, Chile

January 27, 2022

**Abstract**

In mountain areas, long-term snow avalanche risk evaluation is of paramount importance for land use planning. In avalanche-prone areas, when real estate demand is high, for instance, building protective structures may be a sensible choice for reaching a compromise between safety and development. Specifically, minimizing the risk within a quantitative framework can provide optimal defense structure configurations (size, localization, construction technology, etc.). However, existing approaches based on a proper theoretical decision-making framework still suffer from limitations making them hardly usable in practice. It is herein proposed to account for the physical, functional, and monetary dimensions of a protective measure within the assessment of total risk. Total risk, which is calculated as the mean expected loss, is quantified within a four-state system in which the failure of the dam and the failure of the dwellings to be protected are assessed with specific vulnerability relations. Bounds for the risk and subsequent optimal dam design values are quantified using minimum and maximum (min/max) functional efficiency relations of the dam. Additional assumptions regarding the functional-structural efficiency relation allow for the optimal design and corresponding minimum risk to be reached. An application

is proposed with a case study from the French Alps. A comprehensive parametric study shows that the min/max bounds risk quantification is worth implementing in some cases, such as, for instance: if there is a high uncertainty of the functional efficiency of the dam, of if the assets to be protected have a monetary value. However, when the failure of the dam is unlikely to occur (due to its location or to its material resistance), it is shown that quantification of the intermediate risk without the min/max bounds approach is sufficient. In the future, the framework could be extended to many other mountain hazards (debris flows, landslides, etc.), more complex elements at risk, and even to problems going beyond the sole question of land-use planning such as traffic road regulation.

**Keywords:** Risk mitigation; Snow avalanche; Vulnerability; Optimal countermeasures; Functional efficiency.

**Color:** Color should be used in print for Figures 3, 8, 9, 10, 11, 12

# 1 Introduction

## 1.1 Context

Some countries with densely inhabited mountain areas are threatened by snow avalanches. In these areas, there is a need to develop quantitative approaches, such as snow avalanche risk quantification, to manage land use and land occupancy and to set up strategies to lower the short- and long-term risks. Winter periods with heavy snowfall in the past led to avalanches reaching residential buildings, causing major damage and in some instances human casualties. For instance, residential buildings were strongly impacted by snow avalanches that occurred in February 1970 (Fig.1a) and January 1981 (Fig.1b) in the Maurienne valley located in the French Alps. At the European scale, the winter of 1998/1999 was marked by catastrophic snow avalanche events in the entire alpine arc, which reached built environments. The most serious events of this period were: In France, 12 people died inside residential buildings impacted by a snow avalanche in Montroc village on February 9; in Switzerland, 12 people died and extensive property damage was reported in Evolène (canton of Valais) on February 21; and in Austria, 38 people died and with major property damage being reported in Galtür on February 23. More recently, on January 18, 2017, the Rigopiano avalanche struck a hotel in Italy, where 29 people died (Frigo et al., 2018, 2021). Other avalanche events in the past did not cause fatalities but resulted in heavy damage to residential buildings (e.g., in December 2008, in southern France; Gaucher et al. (2010); Eckert et al. (2010a)).


Figure 1: Examples of damage caused by snow avalanches to residential buildings in the Maurienne valley located in the French Alps: (a) on February 24, 1970, in Lanslevillard, Savoie, France (Photo credits: ©Section d'étude des troupes de Montagne, Chef de Bataillon Talon (1970)); (b) on January 20, 1981, in Saint-Colomban-des-Villards, Savoie, France (Photo credits: ©François Valla/INRAE).

In avalanche-prone areas and within the operational context, hazard intensity and occurrence are quantified via the analysis of several scenarios, which are then used as a proxy of the risk and as aids to guide the implantation of protective measures. However, certain limitations of this kind of approaches were pointed out by Eckert et al. (2018), such as for instance: 1) the reference hazard, which is generally based on a given return period, is impossible to define on the basis of deterministic numerical methods only, requiring additional ad-hoc assumptions to determine its probability; 2) it does not explicitly account for exposure (only hazard is considered explicitly); and 3) there is no potential non-linearity between hazard magnitude and damage level, e.g., a vulnerability relation. In the research context, snow avalanche risk quantification is commonly tackled via approaches closer to statistical theoretical definitions, such as the quantification of expected consequences, following the utility theory based on von Neumann and Morgenstern (1953). In order to bridge the gap between the two contexts, the aim of this article is to propose a decisional framework that is both applicable in the operational environment and grounded on theoretical research developments, taking into account recent works on fragility derivation and the possibility that protective measures do not fulfill their protective purpose.

## 1.2 Current risk quantification approaches

In the field of natural hazard engineering research, risk is usually quantified via the evaluation of exposure, hazard, and vulnerability. Regarding snow avalanches, hazard quantification has been by far the most studied among these three quantities, via studies focusing on triggering processes (e.g., Van Herwijnen et al. (2016); Gaume et al. (2018); Puzrin et al. (2019)), propagation analyses (e.g., Naaim (1995); Barbolini et al. (2000); Gaume et al. (2019)) and runout characterization within the stopping zone (e.g., Lied and Bakkehøi (1980); Ancey et al. (2004); Lavigne et al. (2017)). Comparatively, exposure (e.g., Fuchs et al. (2015)) and vulnerability have been less studied. Indeed, a few research studies have assessed the vulnerability to snow avalanches of buildings (e.g., Papathoma-Koehle et al. (2012)), people (e.g., Keylock and Barbolini (2001)), or protective structures (e.g., Daudon et al. (2013)). However, it was shown that risk quantification demonstrates a high sensitivity to vulnerability relations (Favier et al., 2014b), which justifies strengthening the consideration of vulnerability calculations for both the protective measure and the dwellings to be protected in risk assessment. When individual risk is calculated (such as annual risk of death, serious injury, or loss to which specific individuals are exposed), it is often presented in a mapping framework (Keylock et al., 1999; Cappabianca et al., 2008). Such mapping results could be used as tools to manage land use and land occupancy or to lower the risk of existing assets by finding out that one configuration of protective measures is the best option among various protective strategies. For instance, Rheinberger et al. (2009) found that a hybrid strategy, which combines organizational and physical mitigation measures is well suited for snow avalanche risk management in traffic roads. The optimal design of structural engineering protective measures has already been tackled in a risk framework (Eckert et al., 2008, 2009, 2012; Favier et al., 2016) under the assumption of a never-collapsing protective measure. In Switzerland, a practical tool has been developed to quantify the mean expected damage with and without protective measures (Bründl et al., 2015) for natural hazards such as avalanches, torrential floods, or rockfalls . However, in none of the previously described risk approaches was the failure of the protective measures considered.

## 1.3 Protective measure damage and functional models state of the art

Past experiences have shown that protective measures can fail when subjected to certain snow avalanche scenarios (e.g., avalanche-deflective walls in Berthet-Rambaud et al. (2007), avalanche-retaining dam in Barbolini et al. (2009), snow-supporting structures in Margreth (2019)). Indeed,

snow avalanches apply pressure on structures (Thibert et al., 2008; Thibert and Baroudi, 2010; Sovilla et al., 2016), which can lead to various damage levels, i.e., from partial to total collapse (De Biagi et al., 2015). For instance, some of the protective measures of the Taconnaz protective device were found to be in various levels of damage during the winter of 2005/2006 (Fig. 2). Currently, quantitatively assessing the effect of countermeasures in reducing hazard intensity and occurrence is based on the assumption that the dam has not experienced physical damage and is always fulfilling its protective role. For instance, experimental approaches via laboratory studies provide empirical relations to quantify the runout length decrease function of the design of a given protective dam (Hákonardóttir et al., 2003; Faug et al., 2008). After a snow avalanche event, the structural states of each dam are determined in a straightforward manner by expert visual examination; however, the functional efficiency of the damaged dam is rarely defined after the event and uncertainties remain regarding fulfillment of its protective role during the event when structural damage is observed (e.g., did the dam fulfill its functional protective role even if it is assessed as being structurally damaged after the event?). Recent research works proposed using numerical calculation via Finite Element Modeling (FEM) together with reliability algorithms to reproduce and predict the damage to structures in the snow avalanche context (Bertrand et al., 2010; Ousset et al., 2015; Favier et al., 2014a; De Biagi et al., 2016; Favier et al., 2018). In Ousset et al. (2016), the damaged state of the dam was quantified via FEM and via a single degree of freedom model, which was metamodeled through a chaos polynomial expansion (PCE) approach in order to decrease the run-time consumption of the model. In particular, a time-efficient computation is obtained using the Least Angle Regression Sparse (LARS) algorithm, which provides the PCE. Casting the models within a reliability framework made it possible to obtain fragility curves for the protective measure, i.e., the probability of the protective measure collapsing conditioned to the intensity of the snow avalanche expressed in snow avalanche pressure (Ousset et al., 2015). In the end, the physical damage of protective measures was observed and modeled, but the resultant functional issues were still poorly known.

### 1.4 A lack of protective device failure consideration in risk assessment

Risk assessment regarding the failure of protective measures applied to natural hazards in mountain environments has not been studied extensively. Ballesteros Cánovas et al. (2016) applied models of the life-cycle performance of structures subjected to multiple deterioration mechanisms (e.g.,

Sanchez-Silva et al. (2011)) due to debris flows. The approach consisted in integrating the failure effects of extreme events and the progressive degradation affecting torrential protective structures in a risk assessment framework. For instance, torrent check dams for debris-flow protection are subjected to successive events and periodic draining maintenance is regularly needed to remove debris that is trapped above the protection. Thus, it is very important to consider the maintenance costs for periodic draining. Regarding rockfall hazard, a rockfall gallery failure has already been introduced into rockfall risk calculation by Straub and Schubert (2008): The calculation took into account structural failure but did not take into account any costs, neither functional failure nor optimal design study. Awareness regarding the protective role of forests in gravitational natural hazards has increased in the past few decades (Berger and Rey, 2004; Brang et al., 2006; Moos et al., 2018), for rockfall engineering protection purposes (Dorren et al. (2007); Dupire et al. (2016)) or snow avalanches (Bebi et al., 2009). For snow avalanches, the forest can play two protective roles depending on where it is situated: 1) it can be an obstacle in the path of the avalanche (Anderson and McClung, 2012; Takeuchi et al., 2011), and 2) a snowpack stabilizer preventing the initiation of large slabs in release areas (Viglietti et al., 2010; Teich et al., 2012). However, Moos et al. (2018) stated that although the evolution of the protective effect of forests after disturbances has been widely analyzed (i.e., events that decrease the protection capacity of forests such as wind storms or gravitational hazardous processes), there is still no study that takes into account these disturbances and the modifications induced in protection capacity in risk models. Passive protective measures for snow avalanches are usually placed at low altitudes, where snow material infilling is unlikely to occur without a large snow avalanche event, and draining maintenance is usually not planned, contrary to debris-flow events. When dealing with the effectiveness of mitigation measures against snow avalanches, upwards infilling of snow avalanche protective measures is sometimes seen as a serviceability issue threatening the effectiveness of the measure (Margreth and Romang, 2010), its structural safety, and its durability. To the authors' knowledge, no attempts have been made to quantify the influence of the failure of snow avalanche protective measures on the basis of risk within detailed risk quantification approaches.

### 1.5 Overview of the work done

In what follows, a methodology is presented to quantify long-term snow avalanche risk considering a protective dam and its potential failure. Structural damage, functional efficiency, and costs are


Figure 2: Overview of damage caused by a snow avalanche to different elements of the Taconnaz reinforced concrete structure during the winter of 2005/2006. Damage intensity is sorted in four states: (a) without damage; (b) fully destroyed; (c) partially destroyed; (d) with cracks (Photo credits: ©François Rapin/INRAE).

addressed. The risk for a given studied element is quantified by integrating the distribution of the avalanche hazard for various dam designs. Quantification of snow avalanche hazard consists in determining the distribution of the flow heights and velocities at any abscissa in the avalanche path, the distribution of the runout distances, and the frequency of occurrences within the avalanche path considered. For the sake of simplicity, the residential area is reduced to one building to be protected. The protective measure and the building to be protected can be in two states of physical damage, i.e., undamaged or fully destroyed, and for each damage state, a loss of value is allocated. Thus, the dam-building system is composed of four states: both the dam and the building are undamaged, either the dam or the building is damaged, both are damaged. In order to take into account the structural damage states, fragility curves were used. Various efficiency relations are tested, which

are expressed as a function of the structural state of the dam through a single parameter $h_{eff}$ quantifying the structural-functional relation. Losses are quantified with an economic approach. The main output is to build risk curves depending on the dam height for each of the functionality relations proposed through the quantification of $h_{eff}$. Figure 3 sums up the general idea of the approach. The study is composed of three blocks: 1) the snow avalanche hazard (first column entitled "Avalanche" of Fig. 3), 2) the functional and structural response together with the associated loss of the protective measure ("Damage state", "Functional efficiency", and "Loss" of the "Protective measure" column of Fig. 3, respectively), and 3) the structural response and loss of the building to be protected ("Damage state" and "Loss" of the "Building to protect" column of Fig. 3, respectively). Note that in Fig. 3, a line referring to a "partially damaged" state is included: this "partially damaged" state is not explicitly taken into account hereafter in the calculations but exists in reality. It is indirectly considered in the calculations via the probabilistic estimation of two damage states (conditioned to a given snow avalanche intensity). Also, even if the formal framework throughout the paper is mathematically continuous, the calculation was made considering discretization through the integration over $N$ avalanche scenarios for which $M$ chosen dam heights were tested. Besides, in order to ensure the convergence of the risk results obtained by discretization, Monte Carlo error quantification was performed. Bounds for the risk, which is calculated as the mean expected loss, are proposed based on the minimum and maximum functional efficiency of the dam. An additional intermediate annual risk value is quantified when it is assumed that the dam does not necessarily fully lose its functional role even if damaged. Optimal designs are obtained for each risk quantification configuration. Figure 4 provides an overview of the risk quantitative computational steps in a flowchart. The article comprises four sections on: presentation of the theoretical integrated framework to design optimal countermeasures (Sec. 2), a numerical application (Sec. 3), the main results (Sec. 4), and the discussion, conclusion, and outlook (Sec. 5).

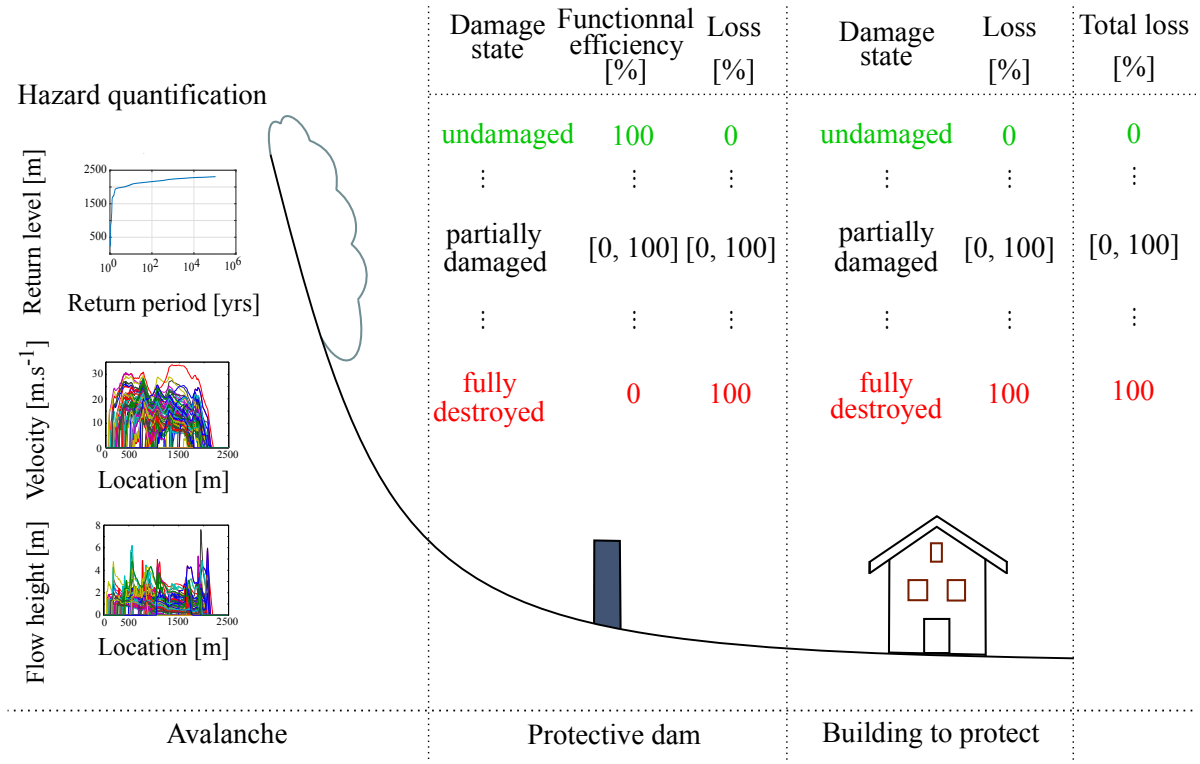


Figure 3: Schematic overview of the approach: 1) the first column corresponds to the hazard quantification, i.e., quantification of the release frequency of snow avalanches and of their velocity and flow depths, spatiotemporal fields on site (the latter are resumed to their maximal values on a 2D topography); 2) the second column corresponds to the estimation of the structural failure via an assessment of damage state, the evaluation of the functional protective efficiency, which is a function of the damage state, and the economic losses of the protective dam, which is also a function of the damage state; 3) the third column corresponds to the estimation of structural failures and the resultant economic losses of the building at stake; and 4) the last column corresponds to the calculation of total losses. The green text is the best-case scenario and the red text is the worst-case scenario.

# 2 A framework for risk and design quantification of optimal countermeasures considering the vulnerability of both the countermeasure and the building at stake

## 2.1 Risk quantification of the dam-building system

### 2.1.1 Physical failure of the dam-building system

The system under study is composed of the protective measure, e.g., a protective dam, and the element at risk to be protected, e.g., an asset at stake such as a residential building. When a snow avalanche reaches the system with a given intensity, it is assumed that the dam, and the building,

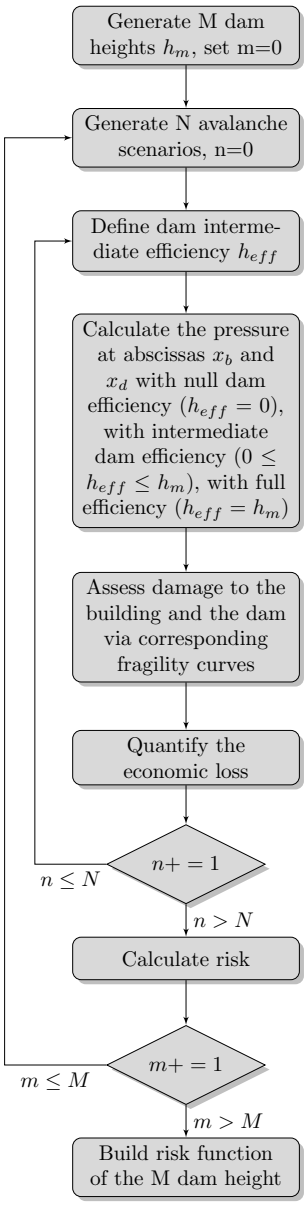


Figure 4: Flowchart of the risk quantification framework. As stated in the text, the risk for a given studied element is quantified by integrating over $N$ avalanche scenarios for each of the $M$ chosen dam heights, for which an efficiency is determined by $h_{eff}$, i.e., a fictitious height that simulates the decrease in the dam protection efficiency when damaged. The optimal dam height is obtained by minimizing the risk function of the M dam height. Operator $x+ = y$ means $x = x + y$. An optimal dam height minimizing losses can then be determined for each functional-structural relationship.

can only be in one of the two following physical states, also called "damage states": undamaged or fully collapsed. The physical state of the dam, written $DS_d$, equals 0 if the dam is undamaged and 1 if fully collapsed. The physical state of the building, written $DS_b$, equals 0 if the building is undamaged and 1 if fully collapsed. The space of possible states of the system is defined by the combination of the previous states: $\Omega = \{(DS_d = 0; DS_b = 0), (DS_d = 0; DS_b = 1), (DS_d =$

$1; DS_b = 0), (DS_d = 1; DS_b = 1)\}$.

### 2.1.2 Structural damage

Physical failure is quantified as the structural damage state of the element studied, i.e., element $d$ when the dam is considered and element $b$ when the building at stake is considered. The probability of failure for each element is defined by its own specific fragility curve. The fragility $V_d(y_d)$ (resp. $V_b(y_b)$) provides the probability for the dam $d$ (resp. the building $b$) to physically surpass a given damage state $ds$ knowing the intensity $y_d$ (resp. $y_b$) of the event reaching the dam (resp. the building):

$$V_{\{d,b\}}(y_{\{d,b\}}) = P(DS_{\{d,b\}} \geq ds | y_{\{d,b\}}), \tag{1}$$

where $DS_d$ (resp. $DS_b$) is the aleatory damage state of the dam $d$ (resp. the building $b$) given the intensity $y_d$ (resp. $y_b$) of the event reaching the dam (resp. the building). Herein, as expressed before, only two damage states are considered, i.e., undamaged without any failure or fully collapsed with failure. The interpretation of a fragility curve is summarized in Figure 5, i.e., the fragility curve expresses a probability of physical failure given the value of the snow avalanche intensity measure, for instance, the pressure.

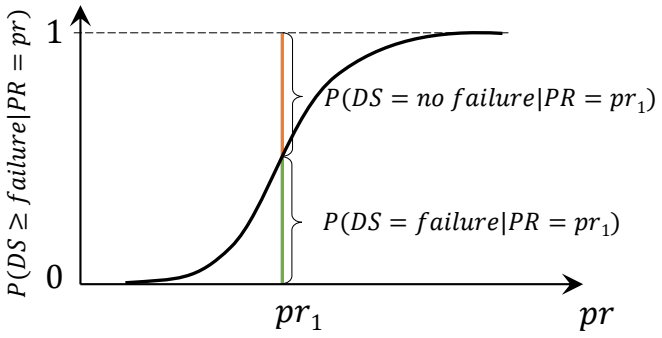


Figure 5: Interpretation of the fragility curve of a structure with two damage states (i.e., either with failure or without any failure), as a failure probability function of the impact pressure, which is later detailed and quantified in Sec.3. Notation $DS$ stands for damage state, where $DS = \{$failure, no failure$\}$, and $PR$ stands for pressure.

### 2.1.3 Risk quantification as a monetary loss

The loss is expressed in monetary value. Then, the risk, expressed in current €, is calculated as the mean expected loss over the amortizing period $T$. Even if alternative quantile-based risk measures are

now emerging (Farvacque et al., 2021), this remains by far the most standard approach for natural hazards. This classic risk measure assumes that the protective system, and thus the residential building to be protected, is rebuilt identically in the case that it has suffered any damage after a snow avalanche event. The actualized total loss of the system is the sum of the initial cost of the countermeasure, e.g., the dam construction cost at year one, $C_0 h_d$, the dam mean reparation cost over the amortizing period, $\lambda A C_0 h_d \int_{\Omega_{y_d}} V_d(y_d) p(y_d) dy_d$, and the mean residential building cost over the amortizing period, $\lambda A C_1 \int_{\Omega_{y_b}} V_d(y_b) p(y_b) dy_b$. This yields:

$$R = C_0 h_d + \lambda A C_0 h_d \int_{\Omega_{y_d}} V_d(y_d) p(y_d) dy_d + \lambda A C_1 \int_{\Omega_{y_b}} V_d(y_b) p(y_b) dy_b, \tag{2}$$

where $C_0$ [€.$m^{-1}$] is the linear cost of the protective dam, $h_d$ [$m$] is the height of the protective dam, $\lambda$ [$year^{-1}$] is the annual rate of snow avalanche occurrence, $C_1$ [€] is the cost of the element to be protected, e.g., the residential building, $A$ [.] is the actualization rate and is calculated over the amortizing period $T$ expressed as

$$A = \sum_{t=1}^{T} d(t), \tag{3}$$

where $d(t)$ is a current value factor for the year $t$, the subscripts $d$ and $b$, respectively, refer to the protective dam and the residential building, $y_x$ refers to the avalanche intensity characteristics such as the velocity, density, and height of the flow affecting element $x$, and $p(y_x)$ refers to its distribution. Note that Eq 2. which describes the behavior of the avalanche-dam-building system is extremely general, almost independent of any choice of statistical or deterministic model, and potentially applicable to many risk mitigation problems. The only underlying assumption is in fact that the considered system can be realistically described with the four states of the $\Omega$ space.

### 2.1.4 Considering the functional efficiency of the dam in the risk quantification

In Equation 2, the mean residential building cost over the amortizing period is quantified as $\lambda A C_1 \int_{\Omega_{y_b}} V_d(y_b) p(y_b) dy_b$, where $y_b$ is the intensity of the avalanche at the building position, $x_b$. The intensity of the avalanche at position $x_b$ is a function of the initial magnitude of the avalanche and the efficiency of the protective measure to weaken the avalanche intensity. Herein, it is assumed that if the dam resists the avalanche impact, the efficiency of the dam is linked to its original height $h_d$. In that particular case, the intensity at the building location is a function of $h_d$: $y(h = h_d)$. However, if the dam collapses, the efficiency is not known and it is herein assumed to be linked to an

efficiency height $h_{eff}$, with condition $0 \leq h_{eff} \leq h_d$. In the latter case, the intensity at the building location is a function of $h_{eff}$: $y(h = h_{eff})$. The calculation of the mean residential building loss over the amortizing period can be split into two sub-calculations as a function of the dam efficiency, i.e., a calculation if the dam remains physically unaffected and its efficiency is quantified as a function of $h_d$, and a calculation if it does not remain unaffected and its efficiency is quantified as a function of $h_{eff}$. Equation 2 is then rewritten as:

$$\begin{aligned} R = C_0 h_d + \lambda A C_0 h_d \int\limits_{\Omega_{y_d}} V_d(y_d) p(y_d) dy_d \\ + \lambda A C_1 \iint\limits_{\Omega_{y_d, y_b}} \left[ V_d\left(y_d\right) V_b(y_b(h = h_{eff})) + \left(1 - V_d\left(y_d\right)\right) V_b(y(h = h_d)) \right] p(y_d, y_b) dy_d dy_b. \end{aligned} \tag{4}$$

## 2.2 Bounds for risk depending on the functional efficiency of the protective dam

Bounds for the annual risk are calculated considering different rates of functionality efficiency of the protective dam. The minimum bound for risk is calculated considering the "best-case scenario," i.e., when the dam is destroyed by an event and fulfills its intended protective functional purpose (cf. 2.2.1). The maximum bound for risk is calculated considering the "worst-case scenario," i.e., when the dam is destroyed by an event and loses its functionality of protection (cf. 2.2.2). The destruction rate of the dam is calculated using the fragility curve of the dam.

An intermediate calculation of risk is made considering that when the dam is destroyed by an event, it loses its functionality of protection only partially (if not destroyed, it fulfills its intended protective functional purpose). This intermediate calculation is presented in Section 2.3, where the functionality of the dam after damage is sampled from a distribution or deduced from an analytical relation.

### 2.2.1 Minimum bound for risk

The minimum annual risk bound is quantified when it is considered that the dam can be destroyed and thus needs to be repaired but has fulfilled its functionality purpose. The minimum annual risk is thus calculated as:

$$R_{min} = C_0 h_d \left(1 + \lambda A \overline{V_d}\right) + \lambda A C_1 \int\limits_{\Omega_{y_b}} V_b(y_b(h = h_d)) p(y_b) dy_b, \tag{5}$$

where $\overline{V_d}$ is the expected value of $V_d(y_d)$ over $y_d$, i.e. $\overline{V_d} = \int_{\Omega_{y_d}} V_d(y_d)p(y_d)dy_d$.

### 2.2.2 Maximum bound for risk

The maximum annual risk bound is quantified when it is considered that the failure of the dam implies its inefficiency, i.e., in the calculation, the height of the dam is set to $h = 0$. The maximum annual risk is thus quantified as:

$$\begin{aligned} R_{max} =& C_0 h_d \left(1 + \lambda A \overline{V_d}\right) \\ &+ \lambda A C_1 \iint_{\Omega_{y_d,y_b}} \left[V_d\left(y_d\right) V_b(y_b(h=0)) + \left(1 - V_d\left(y_d\right)\right) V_b(y_d(h=h_d))\right] p(y_d, y_b) dy_d dy_b. \end{aligned} \tag{6}$$

## 2.3 Intermediate risk calculation using additional assumptions regarding the functional-structural efficiency relation

An intermediate annual risk value is possible to quantify if it is assumed that the dam does not necessarily fully lose its functional role even if damaged. As it is an intermediate quantification step (conceptually far from the previous approach of the classic minimum and maximum bounds), several calculation proposals are herein exposed. First, a fictitious height $h_{eff}$ is allocated to the dam height in order to simulate its protection efficiency. It yields:

$$\begin{aligned} R_{interm} =& C_0 h_d \left(1 + \lambda A \overline{V_d}\right) \\ &+ \lambda A C_1 \iint_{\Omega_{y_d,y_b}} \left[V_d\left(y_d\right) V_b(y_b(h=h_{eff})) + \left(1 - V_d\left(y_d\right)\right) V_b(y_b(h=h_d))\right] p(y_d, y_b) dy_d dy_b. \end{aligned} \tag{7}$$

The functional analysis consists in quantifying the efficiency of the dam knowing the physical damage state. The efficiency of the dam is expressed via the value of an effective height $h_{eff}$. This value can be deterministically or stochastically determined knowing the remaining height of the damaged dam, the pressure of the avalanche at the dam abscissa, and the damage state of the dam.

Thus, as a second step, various relations are set to quantify $h_{eff}$. To obtain the value of $h_{eff}$, it is proposed to use the probability of failure conditioned to avalanche pressure, such as:

$$h_{eff}(pr) = h_d \left(1 - p(DS_d = failure | PR = pr)\right), \tag{8}$$

or,

$$h_{eff}(pr) = h_d \left(1 - p(DS_d = failure | PR = pr)\right)^{\beta}, \tag{9}$$

Statistically, one can propose any statistical distribution that is supported on the bounded interval $[0, h_d]$ such as a truncated normal distribution on $[0, h_d]$, a beta distribution defined on $[0, h_d]$ or as considered herein a uniform distribution $[0, h_d]$,:

$$h_{eff}(pr) \sim U(0, h_d). \tag{10}$$

With regards to Eq. 2, Equations 3 to 7 remain rather general. Eqs. 3 and 7 rewrite Eq. 2, computing some integrals and introducing the $h_{eff}$ quantity that materializes the link between structural damage and the functional efficiency of the dam (or, potentially, of another mitigation measure). Eqs. 5-7 introduce some bounds corresponding to the undamaged and fully damaged cases that frame an intermediate "best guess case". Hence, with regards to Eq. 2, the only true additional assumption is that a dam failure cannot increase damages to the building with regards to the original unprotected case, see Sect. 5 for discussion. By contrast, Eqs. 8-10 introduce much stronger assumptions regarding the quantification of the link between structural damage and functional efficiency of the dam. Such assumptions are necessary if one wants to say more than only "the best guess $R_{interm}$ is somewhere in between the bounds".

### 2.4 Optimal design

Risk is quantified to calculate the amount of loss of a system threatened by a given hazard at a given time, e.g., a mean expected value of loss, a standard deviation or a quantile of the value of loss. It can also be calculated in a prospective way, i.e., when adding a protective measure to the system, the optimal design of the protective measure can be defined as the one minimizing the risk. Herein, it is assumed that the search for the optimal design of a snow avalanche protective dam can be summarized as the search for its optimal height. In this framework the optimal design is given by minimizing Eq. 4 over variable $h_d$, or, depending on the functional role given to the protective dam, by minimizing Eq. 5, Eq. 6, or Eq. 7.

# 3 Application

To make the computation of Equations 5-7 feasible, additional modelling assumptions are required regarding avalanche hazard, avalanche dam functional efficiency and vulnerability relations for the dam and the potentially exposed building. Those used in our application are detailed in what follows, but other choices could be used instead within the same formal framework, see Sect. 5 for discussion.

In addition, the application case study is a path situated in the French Alps, in the village Bessans in the Savoie department in the Maurienne valley. It has been described in depth in Eckert et al. (2010b). The main characteristics to be recalled are that the path is 2300 m long from the top of the path to its lower part, with an altitude ranging from 3200 m to 1700 m. Most of the observed avalanches stopped at the end of the path between 1900 m and 2090 m.

## 3.1 Avalanche hazard model

Assuming stationarity of avalanche activity in the path studied, the occurrence of events is assumed to follow a Poisson distribution with parameter $\lambda$. Let us write $\lambda$ the annual rate of occurrence of the avalanche in the given path and $\lambda P(X_{stop_0} \geq x_d)$ the annual rate of occurrence of the avalanche for which the runout $x_{stop_0}$ exceeds abscissa $x_d$. With 41 avalanches observed in 44 years, an estimator of $\lambda$ is 0.93.

Using the statistical-dynamical model developed by Eckert et al. (2010b), the joint distribution of velocity at any abscissa of the avalanche path is known through the generation of a sample, e.g., $p(v(x_d), v(x_b))$. The pressure distribution is deduced assuming that

$$pr = C_x \frac{1}{2} \rho v^2, \tag{11}$$

where $C_x$ is the drag coefficient and $\rho$ the density of the avalanche flow. Note that $C_x$ is considered as a constant in the present study. It can depend on some factors like the obstacle shape ($C_x$ is typically equal to 2 for an impact against a dam) or the snow type (see Barbolini et al. (2009)). More complicated expressions can be used for $C_x$ to take into account some effects that come into play at low velocity flow regimes, for instance associated with materials stored upstream of the dam. This point will be further discussed in Section 5.

### 3.2 Functional efficiency of the countermeasure: pressure distribution with dam

In accordance with previous studies (Eckert et al., 2012; Favier et al., 2016), the energy dissipation relations from Faug et al. (2008) are used herein. Faug et al. (2008) established a relation – proved to be consistent either for small-scale experiments with granular materials or for full-scale avalanche experiments – that relates the overrun length to the speed of the approaching avalanche and the effective height of the catching dam. The energy dissipation relation consists in providing the decrease in the avalanche velocity at the abscissa of the dam of height $h_d$ in the path:

$$\frac{v_{h_d}^2(x_d)}{v_0^2(x_d)} = 1 - \frac{\alpha h_d}{2h_0}, \tag{12}$$

where $h_0$ stands for the avalanche flow height of the reference flow without a dam at the same location, $v_{h_d}(x_d)$ and $v_0(x_d)$ stand for the velocity at abscissa $x_d$ with a dam of height $h_d$ and without a dam, respectively. The above relation is generally valid for flows with relatively high Froude numbers, and is compatible with Eq. 11, in particular when storage effects upstream of the dam are not considered as dominant (see further discussion in Section 5). For any abscissa below the dam in the path, such as $x_b$, it is assumed that the velocity decrease is propagated, keeping its inertial properties such as:

$$v_{h_d}(x_b) = \max\left(v_0(x_b) - (v_0(x_d) - v_{h_d}(x_d)), 0\right). \tag{13}$$

The joint distribution of pressure is hence known for any abscissa and thus particularly for $x_d$ and $x_b$ abscissa with and without a dam, i.e., $p(PR(x_d), PR_{h_d=0}(x_b), PR_{h_d=h}(x_b))$.

### 3.3 Element at risk and physical damage of the dam

Physical failure is assessed via fragility curves. Three fragility curves for each element of the system were considered and are depicted here: in Figure 6a for the protective dam, and in Figure 6b for the building. For the current study, it is considered that the building or the dam can be in only two states (Fig. 5). It was herein assumed that the economic loss of the building is 100% when the building surpasses its elastic structural capacity. The three fragility curves in Figure 6b are defined as follows: the minimum and maximum fragility curves are the minimum and maximum elastic limit state fragility curves (Favier et al., 2014a), respectively, and the intermediate fragility

curve is the one associated with the elastic limit state of a wall with four supported edges impacted by an avalanche (Favier et al., 2014a). The three fragility curves in Figure 6a are defined as follows: the intermediate fragility curve is the one derived in Ousset et al. (2016), and the minimum and the maximum are obtained by multiplying the x-values of the intermediate fragility curve by 0.5 and 2, respectively. By using this numerical trick, the spread of the dam fragility is visually in accordance with the spread of the building fragility, whose derivation was physically grounded. However, their respective pressure ranges are quite different, i.e., ranging from a few kilopascals to 30 kPa for the building fragility, and a few dozen kilopascals to 800 kPa for the dam fragility.

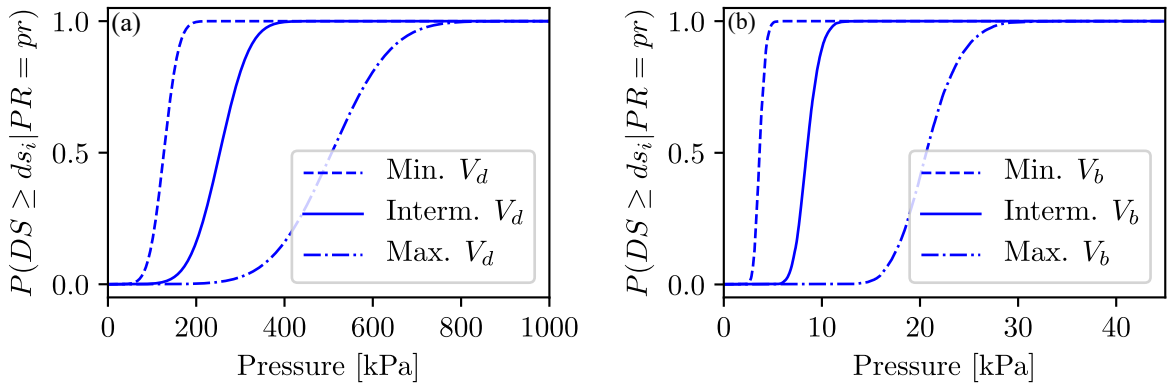


Figure 6: Fragility curves of (a) the protective dam (derived from Ousset et al. (2016)), and (b) the RC building (Favier et al., 2014a).

### 3.4 Loss analysis

The loss analysis consists in calculating the cost for each of the cases previously described. The building that is aimed to be protected costs $C_1$ [current €], the construction of the protective dam is calculated as a linear cost function of the built height $C_0 h_d$ [current €]. Two damage states are considered here in the analysis: without damage or damaged. If either the dam or the building is damaged, the repair cost is set to the construction cost, e.g., the damaged dam is replaced by an identical new dam, whose cost of implementation is the same as the initial construction cost. It should be noted that renovation and maintenance costs have not been explicitly considered, neither the costs such as the loss of human lives inside the building nor the indirect costs (e.g., environmental costs), but these could have been included when quantifying $C_0$ (e.g., adding the cost of human lives to the initial building cost) or $C_1$ (e.g., adding an annually amortized maintenance cost to the initial construction cost). To express future costs in [current €] unit, a current value factor for the year $t$

is calculated as:

$$d(t) = \frac{1}{(1+i_t)^t},$$

where $i_t$ expresses the annual interest – or discount rate – for the year $t$ and is commonly assumed to be steady in time and equal to 4% over the next 50 years.

### 3.5 Default values and parametric study

For seven parameters comprising the risk equations, default values were defined (Tab. 1, Col. 2). Parameters of interest are: the costs of the protective measure and the building ($C_0$, $C_1$), their abscissas ($x_d$, $x_b$), their vulnerability ($V_d$, $V_b$), and the functional efficiency of the protective measure ($h_{eff}$). The last column in Tab. 1 provides the minimum and maximum values for each of the seven parameters in order to run parametric studies.

| Parameters [Unit] | Default values | Parametric study |
|---|---|---|
| $C_0$ [present €.m$^{-1}$] | $10,000$ | $2,000$; $50,000$ |
| $C_1$ [present €] | $5,000,000$ | $1,000,000$; $25,000,000$ |
| $x_d$ [m] | $1,900$ | $1,800$; $2,000$ |
| $x_b$ [m] | $2,125$ | $2,064$; $2,164$ |
| $V_d$ [-] | From Ousset et al. (2016) | Adaptation of Ousset et al. (2016) |
| $V_b$ [-] | From Favier et al. (2014a) | From Favier et al. (2014a) |
| $h_{eff}$ [m] | $h_{eff} \sim U[0, h_d]$ | Eqs. 8, 9 |

Table 1: Default values and parametric study allocated to seven parameters of risk quantification: the costs of the protective measure and the building ($C_0$, $C_1$), their abscissa positions ($x_d$, $x_b$), the vulnerability relations for the protective measure and the building ($V_d$, $V_b$), and the functional efficiency relation for the protective measure ($h_{eff}$).

### 3.6 Monte Carlo convergence analysis

To check that the number of samples of snow avalanche hazard is adequate for quantifying the risk at each dam height $h_i$, the 95% (i.e., $\alpha = 0.05$) confidence interval half-width of the estimated mean expected loss was calculated as:

$$HW_{\alpha,i} = z_{\alpha/2}\frac{\sigma_i}{\sqrt{N}}, \tag{14}$$

where $z_{\alpha/2}$ is the value of the 97.5 percentile point of the standard normal distribution, i.e., 1.96, $\sigma_i$ is the standard deviation of the loss obtained considering the $i^{th}$ dam height, and $N$ is the total number of samples of snow avalanche hazard, i.e., $N = 500,000$. The confidence interval around mean $\mu_i$ is defined as $[\mu_i - HW_{\alpha,i}, \mu_i + HW_{\alpha,i}]$.

# 4 Results and analysis

In this section, the results are presented as follows: Section 4.1 highlights the default case and Monte Carlo convergence results; Sections 4.2, 4.3, 4.4, and 4.5 show how risk quantification and optimal design evolve with the dam and element at risk locations, the costs, the fragility relations, and the dam functional efficiency, respectively; and Section 4.6 points out the dispersion of risk quantification and optimal design values for each of the study cases.

## 4.1 Default case and Monte Carlo convergence results

The risk quantification with default case values (Tab.1) is depicted in Fig. 7a. The intermediate curve is calculated considering the functional efficiency of the dam as a uniform distribution with parameters ranging in $[0, h_d]$. This uniform sampling induces the observed slight noise on the intermediate curve. Minimum and maximum risk curves bound the intermediate curve well. The optimal dam height corresponding to the maximum risk curve is lower than the one from the intermediate risk curve, which is lower than the one from the minimum risk curve, i.e., 14 m$<$ 15.4 m$<$ 21 m. The optimal design values obtained by minimizing the minimum and maximum risk curves (21 m and 14 m, respectively) bound the optimal design from the intermediate curve (15.4 m). The maximum risk curve is computed assuming that physical failure of the dam makes its functional efficiency null. The results show that under the assumption that physical failure of the dam makes its functional efficiency null, the optimal dam height is lower than under the assumption that the dam is always fulfilling its functional protective role.

Monte Carlo confidence intervals calculated from Eq. 14 are depicted in Fig. 7b. Fig. 7b shows that quantifying the risk with 500,000 snow avalanche simulations results in the confidence intervals being very narrow around risk estimates. This latter observation is valid for any of the three risk quantification approaches proposed herein, i.e., quantification of minimum, maximum, or intermediate risk values. Such results argue for having confidence in the risk values analyzed hereafter. In what follows, the Monte Carlo intervals are not shown any further.

## 4.2 Influence of the respective locations of the dam and element at risk

The influence of the dam location is depicted in Fig. 8a. Risk curves with dam locations at $1,800$ m and $1,900$ m display the same general behaviors (i.e., shapes and values are similar), whereas risk

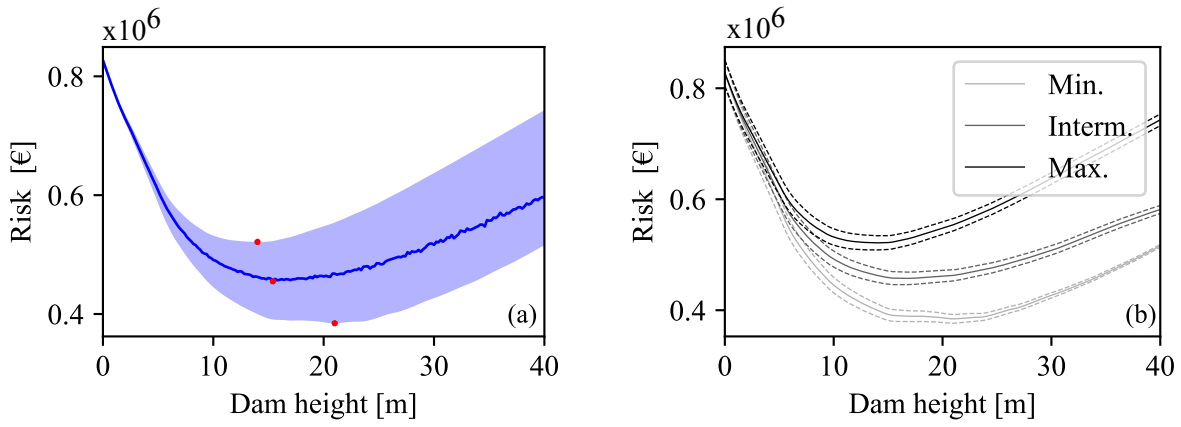


Figure 7: Risk quantification: (a) with default values and relations from Tab. 1 highlighting minimum and maximum risk bounds from Eq. 5 and 6, and intermediate "best guess" value from Eq. 7 with $h_{eff}$ sampled from a uniform distribution $U[0, h_d]$ (red dots point to the minimum values of each risk curve, and the shaded blue area the complete range of possible risk curves between the minimal and maximal bounds); (b) with 95% confidence interval to check Monte Carlo convergence over $500,000$ snow avalanche simulations, where "Min.," "Interm.," and "Max.," stand for the minimum, intermediate, and maximum risk values, respectively, as described in figure (a) here.

curves with dam locations at $2,000$ m follow a different general behavior. Locating the dam at the abscissa $1,800$ m in the path leads to higher risk values than the abscissa $1,900$ m. When assuming a $2,000$-m dam location, minimum and maximum risk curves are mixed up with the intermediate risk curve. Such observations seem to show that locating the dam further down in the path reduces the occurrence of its structural failure. As a consequence, the uncertainty of its functional efficiency plays a smaller role than for the other two locations.

Fig. 8b shows risk curves when the dam is located at default location $1,900$ m and the residential building to protect is located at $2,064$ m, $2,125$ m, and $2,164$ m. Maximum and minimum risk bounds are slightly visible as the general behavior of each curve is controlled by the effect of the building abscissa, which is the steady parameter in this case. The maximum and minimum risk bounds are negligible in the differences in values due to the building abscissa.

### 4.3 Sensitivity to cost values

Figures 9a and b show the sensitivity of risk quantification to dam and building cost values. Throughout the tested cost values, risk quantification is greatly controlled by the assumed cost values, and the influences of the minimum and maximum risk bounds are negligible. For instance, no overlap is observed between minimum and maximum risk delimited areas from each cost value scenario. This latter observation indicates that changing the cost values significantly of either the dam or the

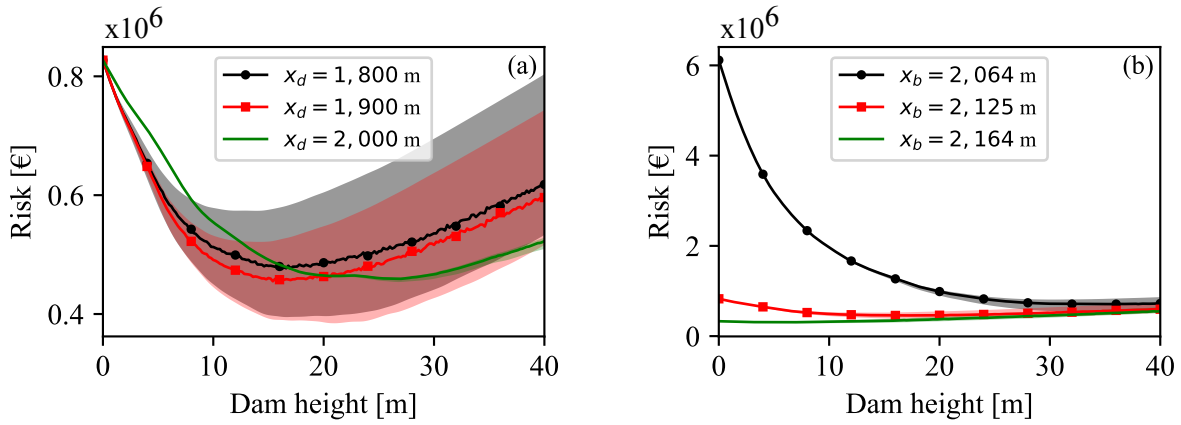


Figure 8: Risk quantification for (a) three positions of the dam, and (b) three positions of the considered building; costs, vulnerability, and dam height efficiency are the default values from Tab. 1.

building to be protected has more more influence on risk quantification than does uncertainty on the efficiency of the protective dam.

In Fig. 9b, risk quantification with building cost value $C_1 = 25,000,000$ € shows a greater absolute minimum and maximum risk bounds width than the two other risk curves related to building cost value. Hence, having uncertainties on the functional efficiency of the dam has more influence when considering a building asset with a very high cost value.

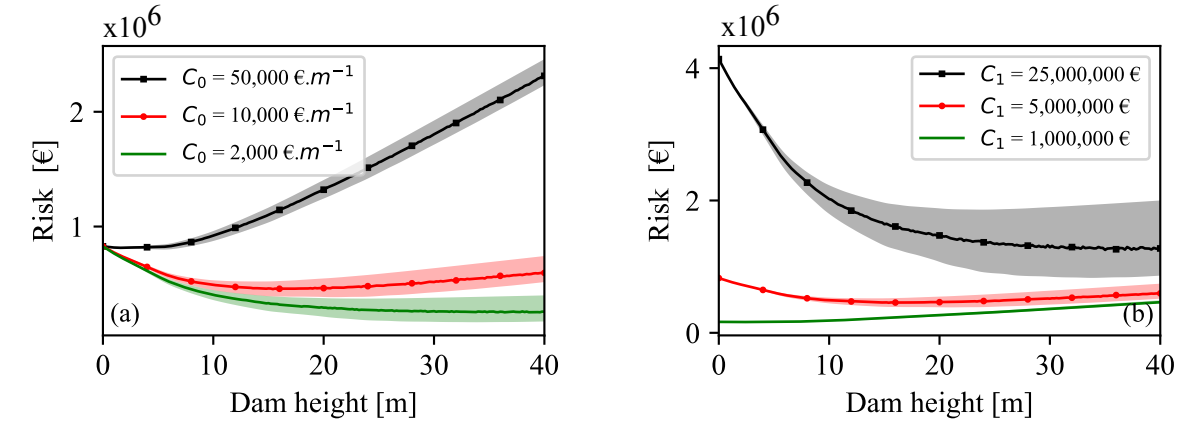


Figure 9: Risk quantification for (a) three values of $C_0$, and (b) three values of $C_1$.

## 4.4 Sensitivity to fragility relations

In what follows the sensitivities of risk to dam fragility curves (cf. Fig. 6a) and building fragility curves (cf. Fig. 6b) are depicted and analyzed via Figures 10a and b, respectively.

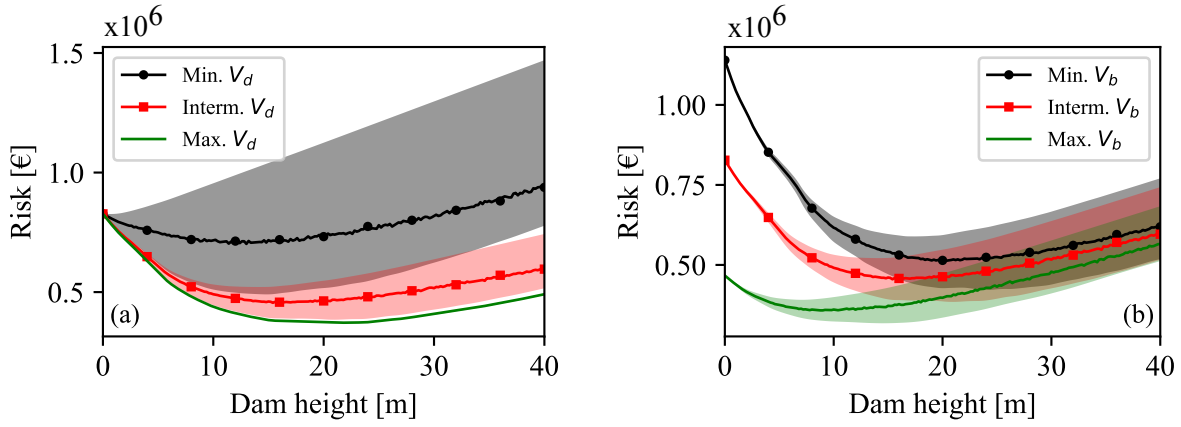


Figure 10: Risk quantification for (a) the three relations of the dam vulnerability, and (b) the three relations of the building vulnerability; costs, position abscissas, and dam height efficiency values are the default ones from Tab. 1.

### 4.4.1 Dam fragility

In Fig. 10a, it is observed that absolute risk bounds are higher for the most "fragile" dam depicted by "Min. $V_d$" curve (i.e., "fragile" is used to characterize the dam with fragility curves having the highest failure probabilities for a given snow avalanche intensity) than the bounds calculated with the two other fragility relations. In fact, the more "fragile" the dam, the greater the difference between the minimum risk and the maximum risk. Furthermore, when the dam is assumed to be very "fragile" and when its functional efficiency is assumed to be null as soon as it fails, the risk curve has a very low dam height optimum. For "the least fragile" dam depicted by "Max. $V_d$" curve (i.e., "the least fragile" is used to characterize the dam with fragility curves having the lowest failure probabilities for a given snow avalanche intensity), the functional efficiency relations do not matter much as long as the dam is nearly never physically damaged.

### 4.4.2 Building fragility

In Fig. 10b, for low values of dam height, the risk is governed by the fragility of the building indicating that it is much higher for more "fragile" buildings. On the contrary, for high dams, the risk is governed by the dam construction cost whatever the building fragility. Hence, similar risk values are observed for high dams, because the dam is sufficiently high to stop nearly all the avalanches before they reach and potentially damage the building at stake. The values of risk at the optimal dam height are in the same order of magnitude for all building fragility considered. The optimal values seem to be sensitive to the building fragility.

### 4.5 Sensitivity to the structural-functional relation

To check the sensitivity of risk and to refine its quantification (cf. Sec. 2.3), it was chosen to use five structural-functional relations, which were derived in order to have simple-to-complex relation types. Figure 11 gathers the risk curves associated with the five structural-functional relations tested. The five structural-functional relations consist in quantitatively linking the effective height of protection of the dam $h_{eff}$ to its original physical height: $h_{eff} \sim U(0, h_d)$, $h_{eff} = h_d/2$, $h_{eff} = h_d \times (1 - V_d)$, $h_{eff} = h_d \times (1 - V_d)^{0.5}$, and $h_{eff} = h_d \times (1 - V_d)^2$.

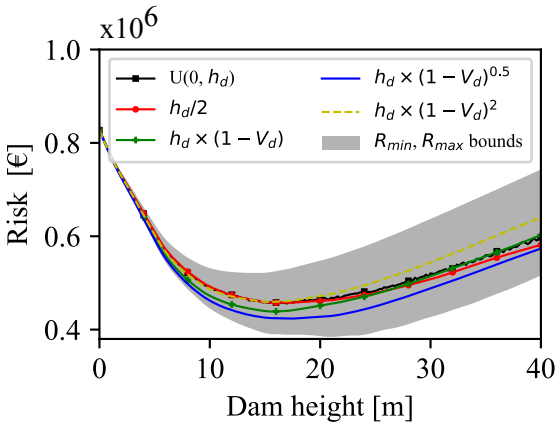


Figure 11: Risk quantification for five structural-functional relations of the dam: $h_{eff} \sim U(0, h_d)$; $h_{eff} = h_d/2$; $h_{eff} = h_d \times (1 - V_d)$; $h_{eff} = h_d \times (1 - V_d)^{0.5}$; and $h_{eff} = h_d \times (1 - V_d)^2$; costs, position abscissas, and vulnerability values are the default ones from Tab. 1.

At first glance, various observations are made. The cases where $h_{eff} \sim U(0, h_d)$ and $h_{eff} = h_d/2$ show similar values of risk, which is logical since $E[X] = h_d/2$ when $X \sim U(0; h_d)$. Hence, when the relation is taken as random, some noise is just added to the same estimate. The case where $h_{eff} = h_d \times (1 - V_d)^{0.5}$ decreases rapidly and presents the lowest values of risk. For high values of dam height, the case where $h_{eff} = h_d \times (1 - V_d)^2$ increases the most rapidly. For high values of dam height, relations $h_{eff} \sim U(0, h_d)$, $h_{eff} = h_d/2$, and $h_{eff} = h_d \times (1 - V_d)$ show similar trends. The exponential cases where $h_{eff} = h_d \times (1 - V_d)^{0.5}$ and $h_{eff} = h_d \times (1 - V_d)^2$ have atypical behavior. For high values of dam height, the non-linearity relations of $h_{eff}$ as a function of $h_d$ seem to influence the risk values. The $R_{min}, R_{max}$ bounds interval proves to be useful here: no matter the chosen link between $h_{eff}$ and $h_d$, and its characteristics, the $R_{min}, R_{max}$ bounds interval provides a robust frame for risk and optimal height values to be used in practice.

### 4.6 Summary of risk and optimal design values as a function of decisional model parameters

For each of the parameters of the sensitivity analysis, risk and optimal height values were collected and are presented in Fig. 12a, and b, respectively. Figure 12c provides a summary of the main trends, which are described below. As a general observation, it is worth noticing that the range of dam heights is congruent to what is implemented as real protective devices in some large avalanche paths (e.g., the two $15-20$ m high deflecting dams of Islandic Flateyri protective device (Jóhannesson, 2001); the 25 m high dam of French Taconnaz protective device (Naaim et al., 2010; Naaim-Bouvet and Richard, 2015)).

Two cases do not show any difference between the minimum and maximum values, neither for risk values nor for optimal design values: $x_d = 2,000$ m and $Max.\ V_d$. Both correspond to cases where the failure of the dam is unlikely to occur: when $x_d = 2,000$ m (i.e., in very low altitudes in the avalanche path, i.e., in the downstream part of the runout zones), overall, snow avalanche intensity is low enough not to trigger the failure of the dam; and when $Max.\ V_d$ is assumed, the dam is "strong" enough not to be destroyed by nearly any snow avalanche intensity occurring.

For $C_0 = 50,000$ €$.m^{-1}$ and $C_1 = 1,000,000$ €, no difference is observed between the minimum and maximum of the risk values, but for the optimal dam height values. The construction of the dam is, comparatively to the building, very expensive for the whole system considered and the optimum is obtained for low values of dam height, with the dispersion in risk values found to be very low. It should be noted that, in both cases, the general behavior of the risk curves is led by the cost of the dam.

The highest dispersion of risk values is observed for case $C_1 = 25,000,000$ €, i.e., for very high building costs. The maximum risk value corresponds to the worst-case scenario, during which the functional utility of the dam is poor, and induces high mean loss values of risk. The corresponding optimal design dam heights are high, meaning that even if the functional response of the dam is poor, it is still worth building a high dam due to the high cost of the building to be protected. This last observation is also made when $C_0 = 2,000$ €$.m^{-1}$, i.e., when the cost of dam construction is much lower than the cost of the building.

The structural-functional relation has a slight effect on the dispersion of risk and optimal design values. However, it is useful to state that whatever the structural-functional relation chosen, an interval for optimal design can be provided: $[14, 21]$ [m], for the default case, $h_{eff} \sim U(0, h_d)$,

$h_{eff} = h_d/2$; $h_{eff} = h_d \times (1 - V_d)$, $h_{eff} = h_d \times (1 - V_d)^{0.5}$, and $h_{eff} = h_d \times (1 - V_d)^2$.

The vulnerability of the building plays a minor role in risk values or in optimal design values (cf. $Min.\ V_b$ and $Max.\ V_b$ in Fig.12). However, assuming that the dam may be "fragile" leads to a wide range of low optimal height values.

515 Eventually, placing the building high in the avalanche path results in a higher risk and optimal design values than placing it in the lower abscissa in the path (i.e., $x_b = 2,164$ m). Placing the protective dam higher in the path than for the default case does not lead to big changes, neither in absolute risk and optimal height values nor in the spread in the range of values.

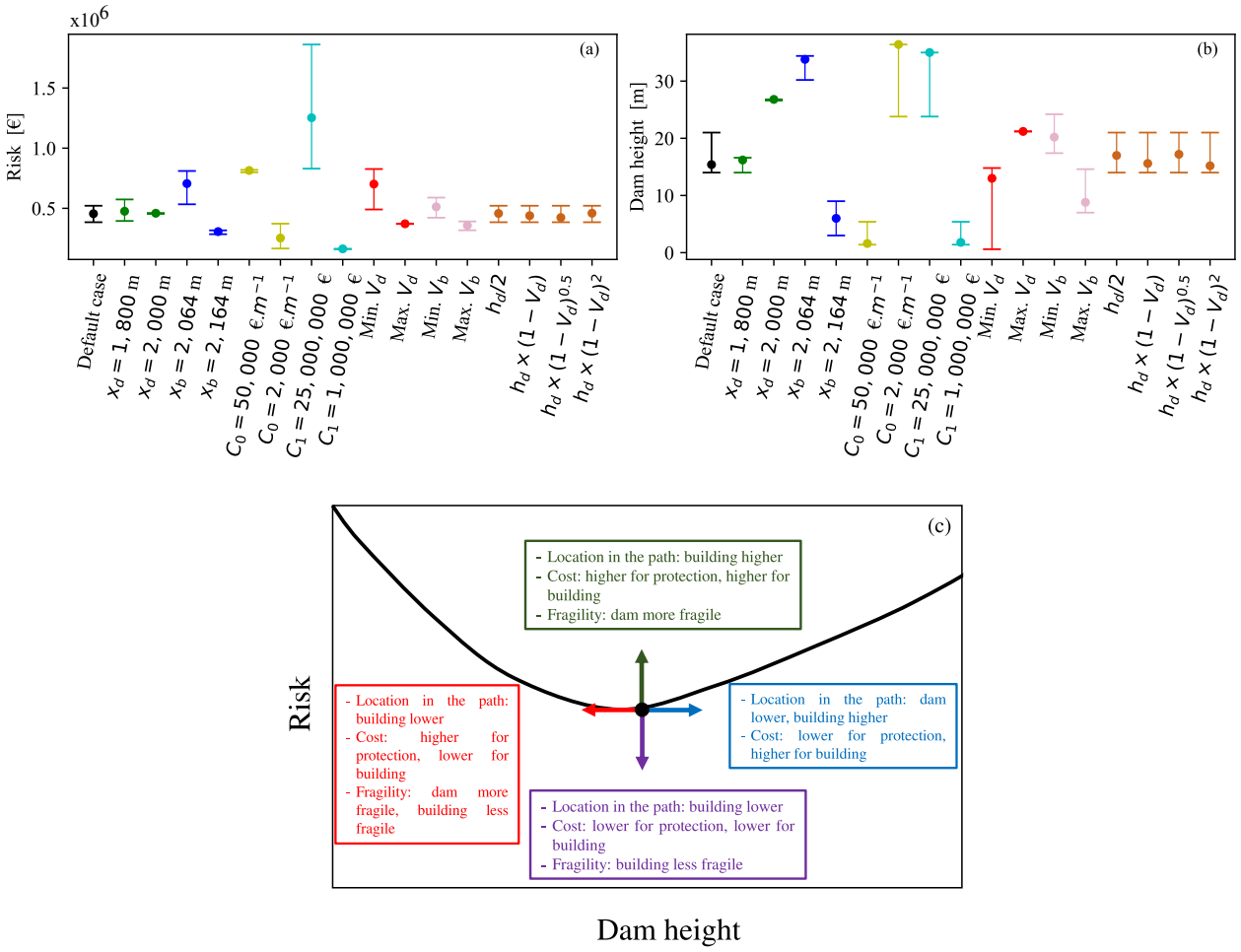


Figure 12: Spread in sensitivity analysis values given by minimum and maximum risk bounds from Eq. 5 and 6, and intermediate "best guess" value from Eq. 7 with $h_{eff} = \frac{h_d}{2}$ for: (a) the minimization of risk, and (b) the corresponding optimal design. Figure (c) summarizes how changes in input variables and relations influence risk and dam optimal height values.

# 5 Discussion, conclusion, and outlook

This article deals with the theoretical framework of quantitative optimization of countermeasures against snow avalanche hazard by minimizing risk, taking into account the structural and functional response of the protective device (a dam). The approach consists in considering the dam-building system to be in one of four physical states after an avalanche occurs: both the dam and the building are undamaged, either the dam or the building is damaged, both are damaged. The risk is quantified as a total cost, which is decomposed into various contributions: 1) the cost of construction of the protective dam, 2) the reparation costs of the dam and building to be protected, and 3) the cost induced by structural damage on the residential building, which is influenced by the functional efficiency of the protective dam. The computational approach proposes to quantify the functional efficiency considering five different structural-functional relations. Bounds for the risk, which are calculated as the mean expected loss, are proposed based on the maximum and minimum functional efficiency of the dam. Thus, the intermediate risk is well framed by the min/max bounds. A comprehensive parametric analysis was conducted to quantify how risk quantification and optimal design evolve with the dam and element at risk locations, the costs, the fragility relations, and the dam functional efficiency.

## 5.1 Main results and new features

On one hand, we showed that if the dam is located relatively high in the path, the min/max bounds approach is worth being implemented as the spread between the bounds is large and thus a range of risk and optimal values are seen. On the other hand, if it is located lower in the path (where it has a low probability of being damaged) the min/max approach is less valuable since the spread between the bounds is very low and thus the range of values offer little information. When the assets to be protected represent a large monetary value, we found that the min/max approach is worth following and provides useful uncertainty bounds. The min/max approach is also worth implementing when the dam is very fragile, because the difference between the minimum risk and the maximum risk is very high. Finally it was illustrated that if the functional relation for the dam is hardly assessable, the bounds intervals provide a safe frame for risk and optimal design values.

In regard to previous works, the proposed risk framework is consistent with the traditional definition of the mean expected loss, which has already been accurately reported in the field of snow avalanche

research. The latest advances that were made on the derivations of fragility curves for snow avalanche protective dams and residential buildings have been integrated here. The novelty of the approach lies in the use of such fragility relations for both the protective dam and residential building, all casted in a very generic unified quantitative risk assessment framwork. Splitting the quantification of snow avalanche risk to consider reparation costs, structural damage, and functional efficiency is innovative where gravitational natural hazards are concerned. The quantification of risk and minimization takes advantage of propagating the uncertainties in the functional relations of the dam: useful bounds are proposed and could be of great interest when the functional efficiency of a protective measure is insufficiently known. However, these bounds were not found to be useful when the dam was planned to be located very low in the avalanche path (i.e., where mainly low-intensity snow avalanche reaches the location) or when the dam was assumed to hardly ever fail structurally.

### 5.2 Limitations due to the functional relations choice

The aim of the article was to propose this novel framework and illustrate its applicability on a real case study. We recall that the modelling of the behavior of the avalanche-dam-building system expressed with Eqs. 2-7 is very general and potentially usable for many avalanche problems and potentially for other issues, see below. However its application requires further statistical and deterministic assumptions to make computations feasible. We therefore made some more stringent choices regarding avalanche activity and its interaction with structures. In the future, other assumptions could be tested, in order to improve the accuracy of the results even more for the tested case, or to implement/study other configurations potentially useful in avalanche engineering. Such potential options are reviewed hereafter. First, the functional relations proposed here assumed that the damaged dam is somewhere between inefficient and fully efficient in fulfilling its protective role. However, one can ask whether a damaged dam would not worsen the intensity of the avalanche scenario. Indeed, if a reinforced concrete dam collapses and "explodes" into several pieces of concrete, the snow avalanche flow would be charged with concrete pieces, and those solid bodies made of concrete could impact and severely damage elements at stake in the path. Perhaps to some extent this latter scenario would be worse than if it had been without concrete pieces and thus dam damage.

### 5.3 Limitations due to the uncertainties on parameters

Second, risk quantification is performed using a collection of numerical sub-models. Hereafter, we criticize the independence assumption of the variables used in the statistical models, the identical rebuilding assumption made when a mitigation strategy is destroyed, and the use of a simplified avalanche-flow interaction law. All parameters are considered to be independent. However, this is not true in practice since some of them may vary simultaneously, e.g., dam construction cost and position, or dam construction cost and its fragility. Furthermore, for each parameter, nominal values are uncertain. Instead of setting a fixed nominal value as it was done here, a statistical distribution could be given to each parameter, in order to take into account epistemic and/or aleatory uncertainties. Another limitation is that the assumption of our model is: after each destructive event, one rebuilds exactly the same elements at risk and establishes the same mitigation strategy. The decision-maker can be described as having a stubborn behavior. In practice, after a destructive event, rebuilding exactly the same configuration is never done, and past examples prove us right (e.g., in the Taconnaz protective site in the French Alps). Yet this is not to be disregarded, since the decision is made conditional to a given state of knowledge. Additional information may lead to a different decision.

### 5.4 Limitations due to hypotheses regarding avalanche regime and activity

Another limitation remains in the use of simplified physics to model the avalanche behavior and the avalanche-flow interaction law. For instance, no storage upstream of the dam was considered here, whereas it was shown that depending on the type of snow and the resulting flow regime (low versus high Froude number flow regime), storage volume can be highly variable and can thus influence the runout characteristics of the snow avalanche downstream of the dam (see Favier et al. (2016) and references therein) as well as the impact pressure. In the latter case, more generalized expressions than Eq. 11 can be used, where the drag coefficient is no longer a constant. $C_x$ is then defined as an equivalent drag coefficient, being the sum of a purely drag coefficient $C_x^0$ and another term that strongly increases when the Froude number $\mathcal{F}$ of the avalanche decreases: $C_x = C_x^0 + k/\mathcal{F}^2$, where $\mathcal{F} = v/\sqrt{gh}$ and $k$ is a kind of earth pressure coefficient associated with the low Froude number (quasi-static) regime. Such a general definition for $C_x$ is well supported by previous studies (Gauer et al., 2008; Faug, 2015; Sovilla et al., 2016) and allows to account for effects such as mass storage upstream of the dam. Furthermore, the statistical-numerical approach and its calibration

on the local data are state of the art but certainly include many approximations and uncertainties. More importantly, the avalanche–dam interaction and its propagation along the topography are represented in a very simplistic way and could be improved in the future. Third, in the current state of knowledge on climate change impacts (Hock et al., 2019), it is known that the assumption of the stationarity of avalanche activity is not accurate (Eckert et al., 2013; Giacona et al., 2021). However, since few studies provide non-stationary parameters to calibrate the Poisson process, it was herein preferred to keep the well-documented stationarity assumption and to state that future improvements of our approach would definitely consider climate change impacts in the avalanche activity.

### 5.5 Final outlooks

As a final comment, it is important to stress that the framework and methodology presented here could in the future be extended to many other other mountain hazards (debris flows, landslides, etc.), more complex elements at risk, and even to mitigation problems going beyond the sole question of land-use planning such as traffic road regulation. The decisional output of the model as a monetary minimization is a realistic variable of interest for stakeholders and is easily transmittable to them. The generality of the approach comes for the minimal assumptions required to express a mitigation problem as a four state system, which easily leads risk bounds and a best guess as functions of a decisional variable (here the dam height), and subsequent minimal costs that can be evaluated within a parametric study. This has been highlighted by the last figure of the article summarizing the parameters of the models that most influence the risk and optimal design outputs, which could be of great value for decision-makers. For instance, previous research works proved that when two rows of braking mounds are installed in an avalanche path, the first line reduces by 20% the kinetic energy and the second by 10% (Barbolini et al. (2009)). Such results are still used as a rule when deciding where to place braking mounds in an operational context. Thus, the work presented here aims to follow the same avenue, i.e., to provide tools and outputs to help decision-making in conditions of a new implementation of a protective dam in a snow avalanche path in the operational context, in the frequent case when finding a good compromise between safety and economic efficiency is an important constraint. From this perspective, implementing different configurations (hazard, functional efficiency and vulnerability models) within the same framework may be seen as a promising issue for novel and useful developments.

**Author contribution** P.F. performed the numerical simulations. P.F. and N.E. developed the theoretical formalism. P.F., N.E., T.F., D.B., I.O., G.C, and J.C.L authors contributed to the final version of the manuscript.

**Competing interests** The authors declare that they have no known competing financial interests or personal relationships that could have appeared to influence the work reported in this paper.

**Acknowledgements** The authors are grateful to the Chilean National Commission for Scientific and Technological Research (CONICYT) under grant Redes 150119 and grant Fondecyt Postdoc 3160483, and the Chilean National Research Center for Integrated Natural Disaster Management (CIGIDEN) under grant CONICYT/FONDAP/15110017 for financially supporting this work. Authors also thank the ECOS-CONICYT Scientific cooperation program project "Multi-risk assessment in Chile and France: Application to seismic engineering and mountain hazards," ECOS170044 and ECOS action C17U02. This work was also supported by the project Cheers Cultural HEritagE Risks and Securing activities (ASP693) co-financed by the Interreg VB Alpine Space Programme through the European Regional Development Fund (ERDF). N. Eckert acknowledges support from the French National Research Agency through the SMARTEN program (ANR- 20-Tremplin-ERC8-0001). INRAE is member of Labex OSUG.

## References

Ancey, C., Gervasoni, C., and Meunier, M. (2004). Computing extreme avalanches. *Cold Regions Science and Technology*, 39(2-3):161–180.

Anderson, G. and McClung, D. (2012). Snow avalanche penetration into mature forest from timber-harvested terrain. *Canadian Geotechnical Journal*, 49(4):477–484.

Ballesteros Cánovas, J., Stoffel, M., Corona, C., Schraml, K., Gobiet, A., Tani, S., Sinabell, F., Fuchs, S., and Kaitna, R. (2016). Debris-flow risk analysis in a managed torrent based on a stochastic life-cycle performance. *Science of the Total Environment*, 557:142–153.

Barbolini, M., Domaas, U., Faug, T., Gauer, P., Hakonardottir, K., Harbitz, C., Issler, D., Johannesson, T., Lied, K., Naaim, M., et al. (2009). The design of avalanche protection dams : recent practical and theoretical developments. *Jóhannesson, T.(editor), Issler, P.(editor), Gauer,*

*P.(editor), Publications Office. European Commission, 212 p., Climate Change and Environmental Risks.*

Barbolini, M., Gruber, U., Keylock, C., Naaim, M., and Savi, F. (2000). Application of statistical and hydraulic-continuum dense-snow avalanche models to five real european sites. *Cold Regions Science and Technology*, 31(2):133–149.

Bebi, P., Kulakowski, D., and Rixen, C. (2009). Snow avalanche disturbances in forest ecosystems—State of research and implications for management. *Forest Ecology and Management*, 257(9):1883–1892.

Berger, F. and Rey, F. (2004). Mountain protection forests against natural hazards and risks: New french developments by integrating forests in risk zoning. *Natural Hazards*, 33(3):395–404.

Berthet-Rambaud, P., Limam, A., Roenelle, P., Rapin, F., Tacnet, J.-M., Mazars, J., et al. (2007). Avalanche action on rigid structures: Back-analysis of Taconnaz deflective walls' collapse in February 1999. *Cold Regions Science and Technology*, 47(1-2):16–31.

Bertrand, D., Naaim, M., and Brun, M. (2010). Physical vulnerability of reinforced concrete buildings impacted by snow avalanches. *Natural Hazards and Earth System Sciences*, 10(7):1531–1545.

Brang, P., Schönenberger, W., Frehner, M., Schwitter, R., Thormann, J.-J., and Wasser, B. (2006). Management of protection forests in the European Alps: an overview. *Forest Snow and Landscape Research*, 80(1):23–44.

Bründl, M., Ettlin, L., Burkard, A., Oggier, N., Dolf, F., and Gutwein, P. (2015). EconoMe - Efficacité et caractère économique des mesures de protection contre les dangers naturels. recueil de formules. `https://econome.ch/eco_work/doc/Formelsammlung_EconoMe_4-0_2016_F.pdf`. Accessed: 2019-12-02 [in French].

Cappabianca, F., Barbolini, M., and Natale, L. (2008). Snow avalanche risk assessment and mapping: A new method based on a combination of statistical analysis, avalanche dynamics simulation and empirically-based vulnerability relations integrated in a GIS platform. *Cold Regions Science and Technology*, 54(3, Sp. Iss. SI):193–205.

Daudon, D., Baroth, J., Ma, Y., Perrotin, P., and Mommessin, M. (2013). Sensitivity of a reinforced concrete protective gallery under a snow avalanche load. *Structural safety*, 41:47–56.

De Biagi, V., Barbero, M., and Borri-Brunetto, M. (2016). A reliability-based method for taking into account snowfall return period in the design of buildings in avalanche-prone areas. *Natural Hazards*, 81(3):1901–1912.

De Biagi, V., Chiaia, B., and Frigo, B. (2015). Impact of snow avalanche on buildings: Forces estimation from structural back-analyses. *Engineering Structures*, 92:15–28.

Dorren, L., Berger, F., Jonsson, M., Krautblatter, M., Mölk, M., Stoffel, M., and Wehrli, A. (2007). State of the art in rockfall–forest interactions. *Schweizerische Zeitschrift fur Forstwesen*, 158(6):128–141.

Dupire, S., Bourrier, F., Monnet, J.-M., Bigot, S., Borgniet, L., Berger, F., and Curt, T. (2016). The protective effect of forests against rockfalls across the french alps: Influence of forest diversity. *Forest Ecology and Management*, 382:269–279.

Eckert, N., Coleou, C., Castebrunet, H., Deschatres, M., Giraud, G., and Gaume, J. (2010a). Cross-comparison of meteorological and avalanche data for characterising avalanche cycles: the example of december 2008 in the eastern part of the french alps. *Cold Regions Science and Technology*, 64(2):119–136.

Eckert, N., Keylock, C., Bertrand, D., Parent, E., Faug, T., Favier, P., and Naaim, M. (2012). Quantitative risk and optimal design approaches in the snow avalanche field: Review and extensions. *Cold Regions Science and Technology*, 79-80:1–19.

Eckert, N., Keylock, C., Castebrunet, H., Lavigne, A., and Naaim, M. (2013). Temporal trends in avalanche activity in the french alps and subregions: from occurrences and runout altitudes to unsteady return periods. *Journal of Glaciology*, 59(213):93–114.

Eckert, N., Naaim, M., Giacona, F., Favier, P., Lavigne, A., Richard, D., Bourrier, F., and Parent, E. (2018). Reflexions on the basis of legal zoning for recurrent mountain risks [repenser les fondements du zonage règlementaire des risques en montagne "récurrents"]. *Houille Blanche*, 2:38–67. [in French].

Eckert, N., Naaim, M., and Parent, E. (2010b). Long-term avalanche hazard assessment with a Bayesian depth-averaged propagation model. *Journal of Glaciology*, 56(198):563–586.

Eckert, N., Parent, E., Faug, T., and Naaim, M. (2008). Optimal design under uncertainty of a passive defense structure against snow avalanches: from a general Bayesian framework to a simple analytical model. *Natural Hazards and Earth System Sciences*, 8(5):1067–1081.

Eckert, N., Parent, E., Faug, T., and Naaim, M. (2009). Bayesian optimal design of an avalanche dam using a multivariate numerical avalanche model. *Stochastic Environmental Research and Risk Assessment*, 23(8):1123–1141.

Farvacque, M., Eckert, N., Bourrier, F., Corona, C., Lopez-Saez, J., and Toe, D. (2021). Quantile-based individual risk measures for rockfall-prone areas. *International Journal of Disaster Risk Reduction*, 53:101932.

Faug, T. (2015). Macroscopic force experienced by extended objects in granular flows over a very broad Froude-number range. *Eur. Phys. J. E*, 38(34).

Faug, T., Gauer, P., Lied, K., and Naaim, M. (2008). Overrun length of avalanches overtopping catching dams: Cross-comparison of small-scale laboratory experiments and observations from full-scale avalanches. *Journal of Geophysical Research: Earth Surface*, 113(F3):1–17.

Favier, P., Bertrand, D., Eckert, N., and Naaim, M. (2014a). A reliability assessment of physical vulnerability of reinforced concrete walls loaded by snow avalanches. *Natural Hazards and Earth System Sciences*, 14(3):689–704.

Favier, P., Bertrand, D., Eckert, N., Ousset, I., and Naaim, M. (2018). Assessing fragility of a reinforced concrete element to snow avalanches using a non-linear dynamic mass-spring model. *Natural Hazards and Earth System Sciences*, 18(9):2507–2524.

Favier, P., Eckert, N., Bertrand, D., and Naaim, M. (2014b). Sensitivity of avalanche risk to vulnerability relations. *Cold Regions Science and Technology*, 108:163–177.

Favier, P., Eckert, N., Faug, T., Bertrand, D., and Naaim, M. (2016). Avalanche risk evaluation and protective dam optimal design using extreme value statistics. *Journal of Glaciology*, 62(234):725–749.

Frigo, B., Bartelt, P., Chiaia, B., Chiambretti, I., and Maggioni, M. (2021). A reverse dynamical investigation of the catastrophic wood-snow avalanche of 18 January 2017 at Rigopiano, Gran Sasso National Park, Italy. *International Journal of Disaster Risk Science*, 12(1):40–55.

Frigo, B., Chiaia, B., Chiambretti, I., Bartelt, P., Maggioni, M., and Freppaz, M. (2018). The January 18th 2017 Rigopiano disaster in Italy–analysis of the avalanche dynamics. In *Proceedings of the International Snow Science Workshop, Innsbruck, Austria*, pages 6–10.

Fuchs, S., Keiler, M., and Zischg, A. (2015). A spatiotemporal multi-hazard exposure assessment based on property data. *Natural Hazards and Earth System Sciences*, 15(9):2127–2142.

Gaucher, R., Escande, S., Bonnefoy, M., Pasquier, X., and Eckert, N. (2010). A look back on the avalanche cycle in Queyras in December 2008. In *Proceedings of the International Snow Science Workshop. Lake Tahoe, USA, 18-22 October 2010*.

Gauer, P., K., L., and Kristensen, K. (2008). On avalanche measurements at the Norwegian full-scale test-site Ryggfonn. *Cold Reg. Sci. Technol.*, 51:138–155.

Gaume, J., Chambon, G., Herwijnen, A., and Schweizer, J. (2018). Stress concentrations in weak snowpack layers and conditions for slab avalanche release. *Geophysical Research Letters*, 45(16):8363–8369.

Gaume, J., van Herwijnen, A., Gast, T., Teran, J., and Jiang, C. (2019). Investigating the release and flow of snow avalanches at the slope-scale using a unified model based on the material point method. *Cold Regions Science and Technology*, 168:102847.

Giacona, F., Eckert, N., Corona, C., Mainieri, R., Morin, S., Stoffel, M., Martin, B., and Naaim, M. (2021). Upslope migration of snow avalanches in a warming climate. *Proceedings of the National Academy of Sciences*, 118(44).

Hákonardóttir, K. M., Hogg, A. J., Jóhannesson, T., and Tómasson, G. G. (2003). A laboratory study of the retarding effects of braking mounds on snow avalanches. *Journal of Glaciology*, 49(165):191–200.

Hock, R., Rasul, G., Adler, C., Cáceres, S., Gruber, Y., Hirabayashi, M., et al. (2019). Chapter 2: high mountain areas. *IPCC Special Report on Ocean and Cryosphere in a Changing Climate*.

Jóhannesson, T. (2001). Run-up of two avalanches on the deflecting dams at Flateyri, northwestern Iceland. *Annals of Glaciology*, 32:350–354.

Keylock, C. J. and Barbolini, M. (2001). Snow avalanche impact pressure-vulnerability relations for use in risk assessment. *Canadian Geotechnical Journal*, 38(2):227–238.

Keylock, C. J., McClung, D. M., and Magnússon, M. M. (1999). Avalanche risk mapping by simulation. *Journal of Glaciology*, 45(150):303–314.

Lavigne, A., Eckert, N., Bel, L., Deschâtres, M., and Parent, E. (2017). Modelling the spatio-temporal repartition of right-truncated data: an application to avalanche runout altitudes in Hautes-Savoie. *Stochastic environmental research and risk assessment*, 31(3):629–644.

Lied, K. and Bakkehøi, K. (1980). Empirical calculations of snow–avalanche run–out distance based on topographic parameters. *Journal of Glaciology*, 26(94):165–177.

Margreth, S. (2019). Effectiveness and maintenance of technical avalanche protection measures in Switzerland. In *International Symposium on Mitigative Measures against Snow Avalanches and Other Rapid Gravity Mass Flows Siglufjörður, Iceland, April 3-5, 2019.*

Margreth, S. and Romang, H. (2010). Effectiveness of mitigation measures against natural hazards. *Cold Regions Science and Technology*, 64(2):199–207.

Moos, C., Bebi, P., Schwarz, M., Stoffel, M., Sudmeier-Rieux, K., and Dorren, L. (2018). Ecosystem-based disaster risk reduction in mountains. *Earth-Science Reviews*, 177:497–513.

Naaim, M. (1995). Modélisation numérique des avalanches aérosols. *La Houille Blanche*, 5-6:56–62.

Naaim, M., Faug, T., Naaim, F., and Eckert, N. (2010). Return period calculation and passive structure design at the Taconnaz avalanche path, France. *Annals of Glaciology*, 51(54):89–97.

Naaim-Bouvet, F. and Richard, D. (2015). *Les risques naturels en montagne*. Editions Quae.

Ousset, I., Bertrand, D., Brun, M., Thibert, E., Limam, A., and Naaim, M. (2015). Static and dynamic FE analysis of an RC protective structure dedicated to snow avalanche mitigation. *Cold Regions Science and Technology*, 112:95–111.

Ousset, I., Bertrand, D., Eckert, N., Bourrier, F., Naaim, M., and Limam, A. (2016). Vulnérabilité d'une structure de protection contre les avalanches de neige en béton armé – Influence des effets inertiels sur les courbes de fragilité. In *JFMS 2016*, pages 1–7. [in French].

Papathoma-Koehle, M., Keiler, M., Totschnig, R., and Glade, T. (2012). Improvement of vulnerability curves using data from extreme events: debris flow event in South Tyrol. *Natural Hazards*, 64(3):2083–2105.

Puzrin, A. M., Faug, T., and Einav, I. (2019). The mechanism of delayed release in earthquake-induced avalanches. *Proceedings of the Royal Society A: Mathematical, Physical and Engineering Sciences*, 475(2227):20190092.

Rheinberger, C. M., Bründl, M., and Rhyner, J. (2009). Dealing with the white death: avalanche risk management for traffic routes. *Risk Analysis*, 29(1):76–94.

Sanchez-Silva, M., Klutke, G.-A., and Rosowsky, D. V. (2011). Life-cycle performance of structures subject to multiple deterioration mechanisms. *Structural Safety*, 33(3):206–217.

Section d'étude des troupes de Montagne, Chef de Bataillon Talon (1970). Fiche concernant le tracé de l'avalanche du 24 février 1970 à Lanslevillard, section d'étude des troupes de Montagne, Bessans, 26 février 1970, Chef de Bataillon Talon. Technical report, Section d'étude des troupes de Montagne. [in French].

Sovilla, B., Faug, T., Köhler, A., Baroudi, D., Fischer, J.-T., and Thibert, E. (2016). Gravitational wet avalanche pressure on pylon-like structures. *Cold Regions Science and Technology*, 126:66–75.

Straub, D. and Schubert, M. (2008). Modeling and managing uncertainties in rock-fall hazards. *Georisk*, 2(1):1–15.

Takeuchi, Y., Torita, H., Nishimura, K., and Hirashima, H. (2011). Study of a large-scale dry slab avalanche and the extent of damage to a cedar forest in the Makunosawa valley, Myoko, Japan. *Annals of Glaciology*, 52(58):119–128.

Teich, M., Bartelt, P., Grêt-Regamey, A., and Bebi, P. (2012). Snow Avalanches in Forested Terrain: Influence of Forest Parameters, Topography, and Avalanche Characteristics on Runout Distance. *Arctic, Antarctic, and Alpine Research*, 44(4):509–519.

Thibert, E. and Baroudi, D. (2010). Impact energy of an avalanche on a structure. *Annals of Glaciology*, 51(54):45–54.

Thibert, E., Baroudi, D., Limam, A., and Berthet-Rambaud, P. (2008). Avalanche impact pressure on an instrumented structure. *Cold Regions Science and Technology*, 54(3):206–215.

Van Herwijnen, A., Gaume, J., Bair, E. H., Reuter, B., Birkeland, K. W., and Schweizer, J. (2016). Estimating the effective elastic modulus and specific fracture energy of snowpack layers from field experiments. *Journal of Glaciology*, 62(236):997–1007.

Viglietti, D., Letey, S., Motta, R., Maggioni, M., and Freppaz, M. (2010). Snow avalanche release in forest ecosystems: A case study in the Aosta Valley Region (NW-Italy). *Cold Regions Science and Technology*, 64(2):167 – 173.

von Neumann, J. and Morgenstern, O. (1953). *Theory of Games and Economic Behaviour*. Princeton University Press.